THE 10 Å TO 7 Å HALLOYSITE TRANSITION IN A TROPICAL SOIL SEQUENCE, COSTA RICA

Christopher Q. Kautz and Peter C. Ryan*

Geology Department, Middlebury College, Middlebury, VT 05753, USA

Abstract—Soils developed on Pleistocene andesitic lava flows and fluvial detritus in the Atlantic coastal plain of Costa Rica display a clay mineral assemblage that includes 10 Å and 7 Å halloysite and lesser amounts of kaolinite and dioctahedral vermiculite. Other secondary minerals include gibbsite, goethite, hematite, maghemite, allophane and amorphous Al hydroxides. Active floodplain soils are dominated by 10 Å halloysite and contain less allophane, while soil clays from Pleistocene terraces consist of a mixture of 10 Å and 7 Å halloysite as well as less dioctahedral vermiculite, kaolinite, and amorphous Al hydroxides. Residual soils formed on Pleistocene lava flows are dominated by 7 Å halloysite with less abundant kaolinite, dioctahedral vermiculite, 10 Å halloysite and amorphous Al hydroxides. This sequence suggests transformations of 10 Å halloysite to 7 Å halloysite and allophane to amorphous Al hydroxides with time. The presence of 10 Å halloysite in Pleistocene terrace soils implies slow reaction rates or metastability.

Quantitative X-ray diffraction (QXRD) analysis indicates a decrease in the amount of plagioclase feldspar from 34 wt.% in the 1–2 year floodplain to 0–1.6% in terrace and residual soils. Plagioclase weathering is paralleled by the formation of dioctahedral clay, allophane and Al hydroxides. Analysis by QXRD also indicates that crystalline minerals comprise 70–95% of the soil fraction, implying 5–30% X-ray-amorphous material. These data are verified by selective extraction using ammonium oxalate, which indicates 8–30% amorphous material. Chemical analysis of the extractant by inductively coupled plasma-atomic emission spectrometry indicates that allophane (Al:Si ratios of 0.92–3.82) occurs in floodplain and some terrace soils while amorphous Al hydroxides appear to coexist with allophane in Pleistocene terrace and residual soils with Al:Si ratios of 6.53–8.53. Retention of Mg to a greater extent than Na, Ca and K suggests Mg incorporation into hydroxide sheets in dioctahedral vermiculite as well as substitution into hydroxides.

Key Words—Allophane, Andesite, Costa Rica, Halloysite, Kaolin, Soil, Terrace, Tropical, Vermiculite, Weathering.

INTRODUCTION

One of the most important controls on clay mineral development is leaching intensity during soil formation (Jackson, 1964; Barshad, 1966; Birkeland, 1969). The 1:1 dioctahedral phyllosilicates, gibbsite and short-range order silicates and hydroxides are among the most commonly formed minerals in humid and tropical climates (Mizota and Van Reeuwijk, 1989; Wada, 1989; Quantin *et al.*, 1991). Halloysite with variable d_{001} values (7–10 Å) and kaolinite are commonly identified 1:1 clay minerals in tropical soils, but the genetic relationship between the minerals remains confused because of high variability in the types and magnitudes of defects that can be present (Brindley and Brown, 1980; Churchman, 1990). Several studies have documented a reduced abundance of halloysite relative to kaolinite with increasing age (Parham, 1969; Eswaran and Wong, 1978; Calvert *et al.*, 1980), yet in other cases researchers have found that kaolinite transforms to halloysite (Robertson and Eggleton, 1991; Singh and Gilkes, 1992). Hughes (1980) documented examples of

weathering sequences where kaolinite increases in abundance at the expense of halloysite, but also cases where halloysite forms at the expense of kaolinite. The work of Delvaux *et al.* (1990) and Watanabe *et al.* (1992) suggested that interstratified halloysite-smectite is an intermediate weathering product in the conversion of 2:1 swelling clays to 1:1 clays and Fe oxides. Righi *et al.* (1999) reported on the formation of kaolinite-smectite (K-S) mixed layers at the expense of basaltic parent material in a temperate climate. The complex and varied nature of weathering products, especially in temperate and humid tropical environments, has created difficulty in the identification of standard weathering sequences of aluminosilicate minerals. This paper reports on a halloysite-rich tropical weathering sequence found in lateritic soils developing on andesitic lava flows and alluvial deposits of similar chemical composition.

STUDY AREA

The study site is located near the town of Puerto Viejo de Saripiqui, Costa Rica, on the grounds of the Organization for Tropical Studies (OTS) La Selva Research Center. Situated at the confluence of two major rivers, the Rio Sarapiqui and Rio Puerto Viejo, the

* E-mail address of corresponding author:
pryan@middlebury.edu

landscape consists of floodplains, terraces and highly eroded bedrock surfaces spanning ~120 m of relief. Lava flows that are primarily andesitic in composition flowed from the central cordilleran volcanic range and periodically covered the entire research area during the Pleistocene epoch (Alvarado, 1990; Sollins *et al.*, 1994). Residual soil profiles formed directly via weathering of these flows are found at higher elevations, while lower-elevation soils have developed on the alluvial deposits of both the Rio Sarapiqui and Rio Puerto Viejo. The mean annual rainfall recorded at La Selva from 1959 to 1985 was 4015 mm and the mean annual temperature was 24ºC (Grieve *et al.*, 1990), classifying the area as tropical wet forest (Janzen, 1983).

MATERIALS AND METHODS

Nineteen soil B horizons were sampled from three different age groups and geomorphic positions: active floodplains (1–2 y, 10 y, 100 y); Holocene to Pleistocene fluvial terraces (Alvarado, 1990); and residual soils. The soils were classified by Sollins *et al.* (1994) as Humid Dystrandept in the lowest terrace set, Andic Humitropept and Typic Humitropept in the middle set and Typic Dystropept in the highest terrace set. Residual soils are classified as Ultisols (Sollins *et al.*, 1994).

In order to limit the effects of dehydration, samples were collected and stored in air-tight plastic bags to prevent moisture loss, and XRD analyses were performed within 24 h of slide preparation. Samples are labeled chronologically. PV-1 is soil from the 1–2 y floodplain, PV-2 denotes the 10 y floodplain, PV-3 is the 100 y floodplain, PV-4 is the youngest terrace, and so on up through soils formed on bedrock, which are denoted PV-15–PV-20 (Table 1).

Samples were prepared for mineralogical and chemical analysis according to the following methods. Bulk soils were wet sieved to remove the >2 mm material (present in only the youngest floodplain). The <2 mm fraction was split, and one sub-sample was settled in Atterburg cylinders to obtain the 2–5 μm and <2 μm fractions for analysis of clay-size mineral content. Oriented sample mounts of 2–5 μm and <2 μm fractions were made for XRD analysis using a Buchner Funnel membrane filtration system with 0.45 μm filters (Drever, 1973). Both the 2–5 μm and <2 μm fractions were analyzed in the air-dried, ethylene glycol-solvated, and heated (250ºC, 1 h; 550ºC) states. The 2–5 μm oriented mounts were also analyzed in formamide-solvated states. Ethylene glycol solvation was achieved through immersion in ethylene glycol vapor at 60ºC for ⩾24 h; formamide was misted onto slides with a fine-mist spray bottle until the clay powder was uniformly saturated.

For all other mineralogical and chemical analyses, another split of the <2 mm fraction was oven dried at 60ºC. For quantitative XRD analysis, 3 g of dried, sieved sample were combined with 0.75 g of corundum (Al_2O_3) and 6–10 mL of water and micronized in a McCrone mill for 10 min to produce a slurry of <10 μm particles. Milled powders were prepared for XRD analysis according to the spray-dry method of Hillier (1999). The best results were obtained by mounting spray-dried powders onto glass slides coated with a very thin film of silicone grease. Peak intensities for quantitative analysis were determined by measuring integrated areas using Jade[®] software (http://www.mdi.com). Reference intensity ratios (RIRs) for each mineral were calculated by: (1) analyzing 50:50 (by weight) spray-dried mixtures of corundum (internal standard) and pure mineral; (2) determining integrated peak area intensities of diagnostic corundum (*e.g.* 2.09 Å) and mineral peaks (see below); and (3) determining ratios of standard:mineral, which were entered into a spreadsheet to facilitate mineral percentage determinations. X-ray diffraction peaks and RIRs used in mineral quantification are as follows: for plagioclase feldspar (quantified as albite), the peak(s) at 3.19–3.21 Å (RIR = 2.0) and the 4.04 Å (RIR = 0.61) for verification; for dioctahedral clay, the peak at 1.49 Å (RIR = 0.21); for quartz, the peak at 4.26 Å (RIR = 0.80) and the peak at 3.34 Å (RIR = 4.1) for verification. Hematite was measured by a relatively sharp 2.70 Å (RIR = 2.0) peak above local background on the low-angle side of the goethite peak at 2.69 Å. Goethite was quantified using the 2.69 Å (RIR = 0.61) peak with the sharp 2.70 Å peak subtracted from its area.

Table 1. Sample identifications, topographic locations and approximate ages of land surfaces on which soils have formed. Ages are from Alvarado (1989) and Nieuwenhuyse and van Breemen (1997). Terraces indicated as Holocene-Pleistocene are either early Holocene or late Pleistocene.

Sample ID	Location	Approximate age
PV-1	Active floodplain	1–2 y floodplain
PV-2	Active floodplain	10 y floodplain
PV-3	Active floodplain	100 y floodplain
PV-4	Low terrace	Holocene
PV-5	Low terrace	Holocene
PV-6	Middle terrace	Holocene-Pleistocene
PV-7	Middle terrace	Pleistocene
PV-8	Middle terrace	Pleistocene
PV-9	Upper terrace	Pleistocene
PV-10	Upper terrace	Pleistocene
PV-11	Upper terrace	Pleistocene
PV-12	Upper terrace	Pleistocene
PV-13	Upper terrace	Pleistocene
PV-14	Upper terrace	Pleistocene
PV-15	Residual soil	Pleistocene (andesite)
PV-16	Residual soil	Pleistocene (andesite)
PV-17	Residual soil	Pleistocene (andesite)
PV-18	Residual soil	Pleistocene (andesite)
PV-19	Residual soil	Pleistocene (andesite)
PV-20	Residual soil	Pleistocene (andesite)

The 4.18 Å goethite peak was not used because of overlaps with the 4.26 Å quartz peak and the kaolin 02,11 peak (4.5–4 Å). Corundum peaks at 2.56, 2.09 and 1.60 Å were used for quantification.

The amount of amorphous or short-range order material (wt.%) in 10 selected samples was determined by ammonium oxalate extraction of the <2 mm fraction (Parfitt *et al.* (1984). 100 mL of 0.2 M ammonium oxalate at pH 3.5 were mixed with 0.5 g of sample and shaken in the dark for 1 h. The remaining solids were separated from the extractant by centrifugation (10 min, 12,000 rpm), dried at 60ºC, and weighed. Major element inductively coupled plasma-atomic emission spectroscopy (ICP-AES) was carried out on the extractant using a Thermo-Jarrell Ash Iris 1000. In addition, major element concentrations in the bulk fraction of these samples were determined by ICP-AES after fusion with lithium metaborate flux (Retallack, 1983; Bestland *et al.*, 1997). Uncertainty determined by replicate analyses and comparison to standards are $\leqslant 3\%$ (2σ, %RSD) for all major elements, except where CaO, K_2O, MgO, MnO and Na_2O values are $< 3\%$, in which case uncertainty is ~5% (2σ, %RSD).

Bulk soil grain-size distributions (<2 mm fraction) were measured in duplicate using a Coulter LS230A (Small Volume Module) Laser Diffraction Particle Size Analyzer after ultrasonic disaggregation with sodium pyrophosphate. Particle morphologies were examined by scanning electron microscope (SEM) analysis of carbon-coated soil aggregates fixed onto Al stubs. Ten soil samples from floodplain, terrace and residual soils were analyzed using a Philips XL20 SEM operating at an accelerating voltage of 20 kv. The spot size varied from 5 to 2 μm depending on the magnification. Energy

dispersive spectroscopy (EDS) was performed using a Princeton Gamma-Tech (PGT) Spirit Energy Dispersive X-ray microanalyzer consisting of a Pentafet light element Si(Li) detector with a crystal cross-sectional area of 10 mm^2. The EDS detector was used in Be-window mode thus allowing the detection of elements no lighter than Na.

RESULTS

Physical properties

Particle-size distribution curves for the full age range of soils illustrate a progressive decrease in particle diameter from the active floodplain to middle terraces (Figure 1), with the percentage of <5 μm material increasing from the active floodplain (6.6%) to the middle terrace set (36.7%). Upper terrace and residual soils display a wide range of <5 μm material (23.2–51.6%) that does not systematically vary with age.

XRD analysis

La Selva soils are composed of both 10 Å and 7 Å halloysite, dioctahedral vermiculite, kaolinite, gibbsite, quartz, goethite, hematite, maghemite and short-range order materials (Figure 2). Plagioclase is clearly evident in active floodplain samples based on distinctive peaks at 6.3, 4.04 and 3.20 Å. Pyroxene also appears to occur in floodplains although overlap of the most intense pyroxene peaks with kaolin and plagioclase peaks makes unequivocal identification difficult, given the current data. Halloysite was identified by basal peaks at 10 Å and 7 Å, a disordered 02,11 peak from 20–26º2θ, the shift of the 10 Å halloysite peak to 7 Å upon heating
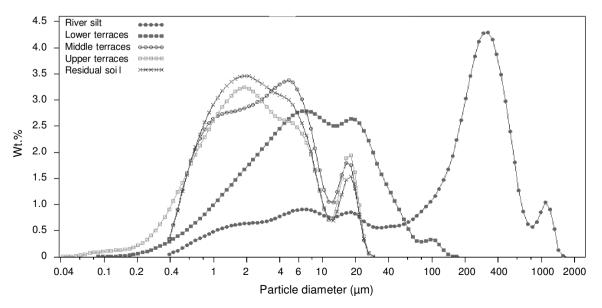

Figure 1. Variations in particle size of soil B horizons as a function of age, as determined by laser-diffraction particle-size analysis.

(250ºC, 1 h), and characteristic response to formamide and ethylene glycol solvation as described below (MacEwan, 1948; Costanzo and Giese, 1985; Churchman, 1990). None of the Fe oxides appears to vary systematically with age. Evidence for dioctahedral vermiculite is presented below. The peak at 4.04 Å in some oriented powders is attributed to small amounts of cristobalite (Moore and Reynolds, 1997), a common constituent of andesitic lavas that has been found in tropical soils (Agbu *et al.*, 1990).

Gibbsite is more abundant in the 2–5 μm fraction than in the <2 μm fraction. Relative abundances of 10 Å and 7 Å halloysite show minor variability among the size-fractions, but the variability is not systematic. Basal kaolin peaks have sharper apices in the 2–5 μm fraction than in the <2 μm fraction, and dioctahedral vermiculite does not vary systematically with size.

Halloysite

Halloysite in active floodplains consists almost entirely of the 10 Å form (Figure 3a). Young, middle and upper terraces are characterized by broad distinct peaks with maximum intensities at 10.0 Å and 7.2 Å (Figures 3b,c). Residual soils are dominated by 7 Å halloysite with only minor amounts of the 10 Å form (Figure 3d).

14 Å minerals

With one exception, ethylene glycol (EG) solvation had no effect on 14 Å peak shape and position, indicating that the peak is not produced by an expandable mineral. The exception is the 1–2 y floodplain (PV-1), which contains a broad 14–16 Å peak that shifts to a broad 17 Å peak upon EG solvation and collapses to

~13.5 Å upon heating to 250ºC (1 h). This indicates the presence of expandable clay in this lowland tropical region, but only in the youngest soil. Incomplete interlayer collapse upon heating (250º C, 1 h) is indicative of high-charge smectite (Moore and Reynolds, 1997). Heating at 250ºC for 1 h also causes a shift of the 14.5 Å peak in non-expandable 14 Å clay to a broader, less intense peak centered at 13.5 Å. In all cases, heating to 550º C for 1 h causes destruction of the 14 Å peak, and formation of a broad peak with maxima at 12, 11 and 10 Å.

These data are consistent with dioctahedral vermiculite with incomplete or poorly-formed Al hydroxide interlayers (Nagasawa, 1978; Starkey *et al.*, 1984). The slight reduction in peak intensity and shift from 14.5 Å to 13.5 Å with heating (250ºC, 1 h) are consistent with the loss of interlayer water (Moore and Reynolds, 1997). Destruction of the 14.5 Å peak and formation of a broad, weak peak centered around 11 Å after further heating (550ºC, 1 h) indicates the dehydroxylation of hydroxy-Al interlayers in dioctahedral vermiculite (Starkey *et al.*, 1984). An alternative interpretation of the 14 Å peak is that it is produced by structural (or chemical) alternation of 7 Å 1:1 layers similar to the alternations described by Chukhrov and Zvyagin (1966). However, loss of water to cause transformation from 14.5 Å to 13.5 Å upon heating (250ºC) is more consistent with a vermiculitic clay than a 1:1 clay. It seems very unlikely that a 1:1 clay could remain intact upon partial loss of the octahedral sheet.

Results of intercalation treatments and heating

Response to ethylene glycol. 10.0 Å peaks (air-dried samples) are absent following EG solvation and the resulting pattern is characterized by weak broad peaks
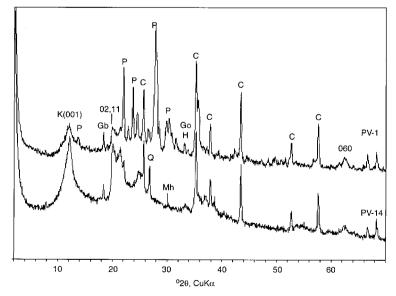

Figure 2. XRD analysis of bulk soils (B horizons) for samples PV-1 (upper pattern) and PV-14 (lower pattern). P = plagioclase, K(001) = 7 Å kaolin peak (halloysite + kaolinite), Q = quartz, C = corundum (internal std), Gb = gibbsite, Go = goethite, H = hematite, Mh = maghemite, 02,11 and 060 are kaolin reflections.
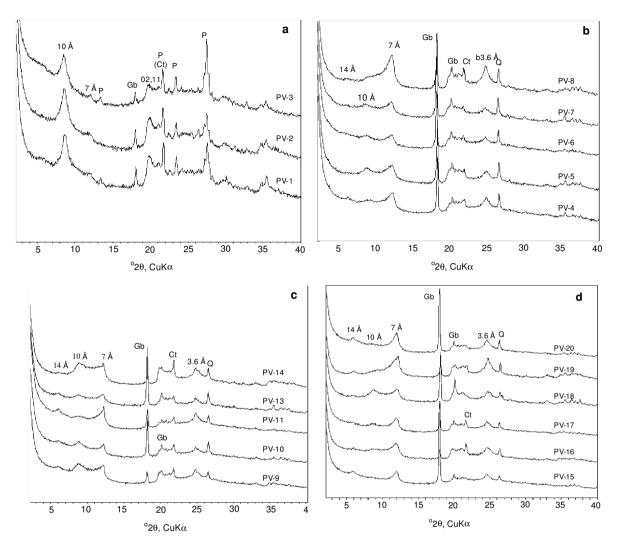
Figure 3. XRD analyses of oriented mounts of air-dried powders, 2–5 μm fraction. Sample numbers are indicated on the right and increase in age upwards. Approximate peak positions are given in Å, P = plagioclase, Gb = gibbsite, 02,11 = kaolin reflections, Ct = cristobalite, Q = quartz. (a) Active floodplains, (b) low and middle terraces, (c) upper terraces, and (d) residual soils.

with maximum intensities at 10.9 Å, 7.2 Å and 3.5–3.6 Å (Figure 4). Kaolin 001 peaks decrease in intensity following EG solvation and kaolin 002 peaks increase in intensity, which is to be expected for halloysite (Hillier and Ryan, 2002). With the exception of clay in the 1–2 y floodplain, which contains an expandable 14 Å mineral, the 14 Å peak is unaffected by EG solvation.

Response to formamide. Formamide treatment results in a weakening of the 7.2 Å peak, loss of the 10.0 Å peak and production of a 10.4 Å peak (Figure 5). In samples containing material of intermediate spacing between 7 and 10 Å, reduction of the 7.2 Å peak is matched by decreased intensity of the broad band between 7 Å and 10 Å. Incomplete shift of 7 Å peaks following forma-mide solvation (~1 h) in all terrace and residual soils

suggests the presence of trace amounts of kaolinite, or incomplete expansion of halloysite layers (Churchman, 1990). The three youngest samples (PV 1–3) showed no evidence of 7 Å peaks following formamide solvation. Formamide intercalation also results in a very broad increased background between ~4.3 and 2.8 Å that partially masks kaolin 02,11 and 002 peaks.

Response to heating. The typical response of all size-fractions to heating (250°C, 1 h; 550°C, 1 h) is demon-strated in Figure 6. In addition to causing the 14.5 to 13.5 Å peak shift, heating to 250°C causes destruction of the 10.0 Å peak while the intensity of the 7.2 Å peak increases markedly. Increased peak intensity at 7.2 Å is matched by increased intensity of the 002 peak at 3.6 Å.

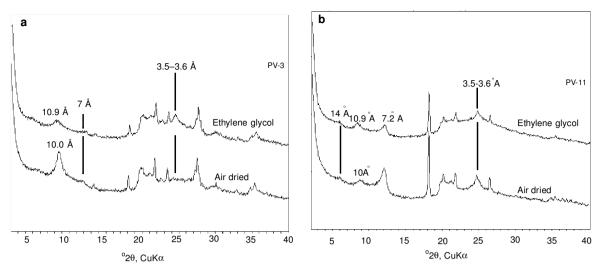Further heating (550°C, 1 h) results in the replace-ment of distinct 14, 10 and 7 Å peaks by a weak broad

Figure 4. XRD analyses of oriented mounts of representative ethylene glycol-solvated powders (2–5 µm fraction). (a) = PV-3, (b) =PV-11.

band between 13 and 8 Å, with maxima at 12, 11 and 10 Å. The gibbsite peak at 4.85 Å is also destroyed. There is an increase in the overall background intensity of the patterns after heating.

Quantitative XRD

Plagioclase ranges from 34 wt.% in active 1–2 y and 10 y floodplains to 15 wt.% in the 100 y floodplain. In terrace and residual soils, plagioclase content ranges from 0 to 1.6 wt.%. 10 Å halloysite is the most abundant mineral in active floodplains (45 wt.%); terrace and residual soils are characterized by varying amounts of coexisting 10 Å and 7 Å halloysite, with the 7 Å form increasing erratically in abundance with age at the expense of the 10 Å form (Figure 3a–d). Dioctahedral clay ranges from 36 to 72 wt.% in B horizons of these soils, and increases erratically with age. Quartz ranges
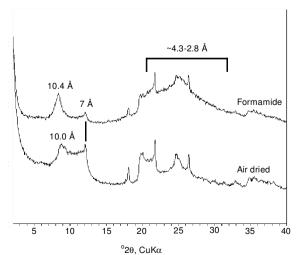
from 1 to 6 wt.%, with lowest concentrations in the modern floodplains. Gibbsite ranges from 2 to 24 wt.% and exhibits no apparent trend with age. The sum of mineral percentages is 70–95%, implying 5–30% amorphous or short-range order materials in these samples (see following section).

Chemical analysis

Ammonium oxalate extraction of amorphous solids. Major element compositions of ammonium oxalate-extractable materials are presented as wt.% oxides in Table 2. Given that loss-on-ignition (LOI) determination is not feasible in this type of extraction, values are normalized to 100% to illustrate trends. Most notable is the increase in Al:Si ratio from 0.92–1.23 in active floodplains (PV-1, PV-3) to 1.92–8.53 in terrace and residual soils. Also notable is the comparison of the
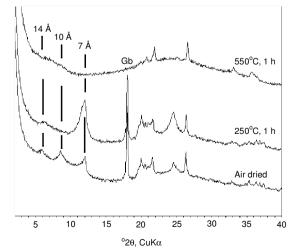

Figure 5. XRD analyses of oriented mounts of formamide-solvated powder (2–5 µm fraction, PV-14).

Figure 6. XRD analyses of oriented mounts heated to 250 ºC and 550ºC for 1 h each (2–5 µm fraction, PV-10). Note the disappearance of gibbsite (Gb) and kaolin (7 Å) at 550ºC.

Table 2. ICP-AES analyses of amorphous material extracted by ammonium oxalate. Results are presented in wt.% oxide, except for Al:Si ratios.

Sample ID	SiO_2	Al_2O_3	Fe_2O_3	MnO	MgO	CaO	Na_2O	K_2O	TiO_2	Al:Si
PV-1	15.71	25.46	47.05	1.73	4.26	0.66	0.84	0.52	3.72	0.92
PV-3	18.98	41.20	31.88	3.31	1.54	0.55	0.73	0.16	1.89	1.23
PV-5	6.29	42.50	34.51	11.11	0.00	1.29	1.16	0.72	2.34	3.82
PV-6	12.32	41.71	30.70	7.03	0.71	2.51	2.34	0.55	1.93	1.92
PV-7	6.29	43.63	32.39	16.50	0.00	0.84	0.83	0.19	1.79	6.53
PV-8	3.14	47.30	46.70	0.27	0.00	0.92	0.57	0.34	0.74	8.53
PV-9	12.32	45.32	34.25	2.00	2.80	1.52	2.16	0.70	1.21	2.58
PV-17	4.59	61.27	29.04	0.64	0.00	1.08	2.01	0.60	0.90	7.56
PV-18	3.83	52.34	38.59	1.10	0.00	0.71	1.98	0.16	1.32	7.74
PV-19	5.46	67.55	20.75	0.05	0.00	1.78	3.36	0.48	0.54	7.01

amount of amorphous or short-range order solids determined by ammonium oxalate extraction to their determination by QXRD. Ammonium oxalate extraction indicates 8–30% amorphous or short-range order solids, whereas QXRD indicates 5–30% (Table 3). Sample-to-sample agreement ranges from excellent (30 *vs.* 30% for PV-7) to poor (8 *vs.* 26% for PV-17).

Bulk chemical composition. Chemical analysis indicates pronounced change in chemical composition with increasing soil age (Table 4). Note the high concentrations of Ca (6.48% CaO) and Na (2.59% Na_2O) in the 1–2 y floodplain and their near absence from middle and upper terrace soils (0.0–0.39% and 0.10–0.28%, respectively). Also notable is the larger amount of Mg compared to Ca and Na in upper terrace and residual soils. Magnesium ranges from 0.19–0.61 wt.% in these soils, whereas CaO and Na_2O are 0.00–0.39 and 0.10–0.15 wt.%, respectively. The increase in Ti content with age reflects the relative insolubility of Ti even in strongly leached soils, and the loss of other soluble elements through chemical denudation (Drever, 1997). Aluminum and Fe generally increase in concentration with age, while Si decreases erratically, but to a much lesser extent than the base cations. Manganese is more concentrated in upper floodplains and lower terraces than in the 1–2 y floodplain, yet it is relatively depleted in upper terraces and residual soils.

Scanning electron microscopy

Kaolin minerals from floodplain, terrace and residual soils occur primarily as nodular and spheroidal particles of ~0.2 µm in diameter (Figure 7). We observed no platy, kaolinite-like crystals. Oval to rod-shaped particles ~0.1–0.3 µm in diameter and up to 2 µm in length (but typically much shorter) occur in all samples but are far less abundant than the nodular and spheroidal particles. Figure 7b depicts the best example of a rod-shaped halloysite particle. There is no apparent systematic difference in halloysite morphology or particle size as a function of soil age (Figure 7a–c). Gibbsite occurs as prismatic crystals with long axes ⩽5 µm (Figure 7d).

DISCUSSION

With increasing age, active floodplain soils and Holocene to Pleistocene fluvial terrace soils exhibit distinctive changes in mineralogical and chemical content. These changes include (1) rapid dissolution of plagioclase feldspar, from 34 wt.% in the 1–2 and 10 y floodplains to 15 wt.% in the 100 y floodplain, and 0–1.6% in terrace and residual soils; (2) leaching of mobile cations, which, ranked from the greatest to least mobility, are Ca>Na>K>Mg>Si; (3) residual concentration of immobile cations Fe, Al and Ti; and (4) transformation of 10 Å to 7 Å halloysite, especially at the

Table 3. Results of mineral quantification by XRD, % amorphous material determined by XRD (% Am-XRD), and % amorphous material determined by oxalate extraction (% Am-OE).

Sample	Quartz	Plagioclase	Goethite	Gibbsite	Halloysite	Sum	% Am-XRD	% Am-OE
PV-1	1.6	34.8	4.2	3.5	46.7	90.8	9.2	17.7
PV-3	0.7	15.4	8.3	3.9	45.9	74.2	25.8	9.5
PV-5	2.8	1.1	1.7	14.1	51.9	71.6	28.4	23.4
PV-6	5.0	0.8	7.5	14.8	42.1	70.2	29.8	21.0
PV-7	5.2	1.9	3.1	23.9	35.8	69.9	30.1	30.0
PV-8	2.8	1.1	1.7	14.1	67.9	87.6	12.4	15.7
PV-9	5.0	2.0	8.5	5.9	65.5	86.9	13.1	12.6
PV-17	2.3	0.0	7.6	4.4	59.9	74.2	25.8	8.4
PV-18	3.1	0.7	6.1	8.4	52.3	70.6	29.4	26.8
PV-19	4.9	1.6	12.4	16.3	59.9	95.1	4.9	15.2

Table 4. Results of ICP-AES analyses of the <2 mm fraction. Data are presented as wt.% oxides.

Sample ID	SiO_2	Al_2O_3	Fe_2O_3	MnO	MgO	CaO	Na_2O	K_2O	TiO_2	LOI
PV-1	48.66	20.12	11.21	0.17	3.49	6.21	2.48	1.89	1.19	4.57
PV-3	43.49	22.67	12.97	0.26	1.52	2.71	1.48	1.23	1.54	12.12
PV-5	29.79	33.81	18.62	0.37	0.26	0.04	0.13	0.25	1.89	14.84
PV-7	25.65	34.11	18.87	0.55	0.26	0.02	0.12	0.25	1.91	18.26
PV-8	32.72	28.72	15.89	0.46	0.22	0.02	0.10	0.21	1.68	19.97
PV-9	41.38	28.20	11.92	0.07	0.06	0.33	0.23	0.26	1.72	15.82
PV-10	30.02	31.38	16.68	0.06	0.32	0.14	0.11	0.16	2.05	19.07
PV-17	34.56	28.96	16.03	0.04	0.14	0.02	0.12	0.10	2.08	17.96
PV-18	32.53	31.73	14.81	0.05	0.19	0.00	0.09	0.09	2.09	18.42
PV-19	27.66	33.45	17.09	0.03	0.19	0.00	0.08	0.09	1.77	19.64

topographic boundaries between the active floodplains and the lowest terrace, and between the highest terrace and residual soils.

XRD behavior of halloysite

The 10 Å and 7 Å peaks from XRD analysis (air-dried samples) indicate coherent diffracting domains of 10 Å and 7 Å halloysite that are produced by a physical mixture of crystals of discrete 10 Å and 7 Å halloysites (Churchman, 1990) and/or partially segregated, intergrown packets of 10 Å and 7 Å layers (Churchman *et al.*, 1972). The saddle between the 10 and 7 Å peaks is attributed to randomly interstratified 10 Å and 7 Å layers as well as partially dehydrated
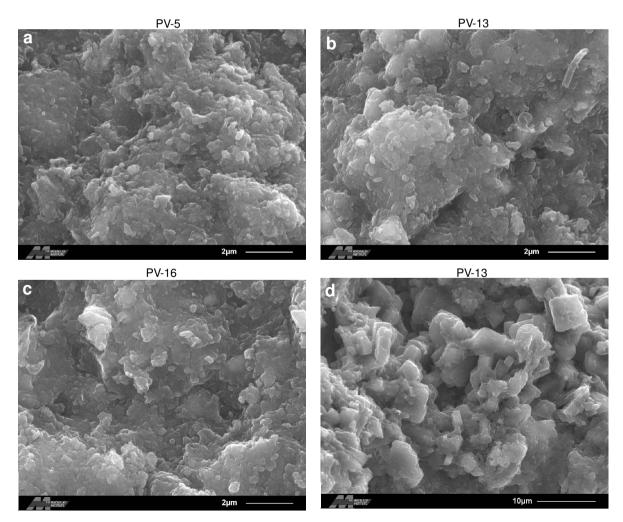

Figure 7. SEM images of halloysite (a–c) and gibbsite (d). Halloysites are from low terrace (a), upper terrace (b) and residual soil (c).

halloysites with spacings of 8.6–7.9 Å (Brindley and Brown, 1980; Costanzo and Giese, 1985). The 8.6–7.9 Å layers could also be interstratified with 7 Å and 10 Å layers, which also would contribute to intensity in this region.

While 10 Å halloysite expands completely to 10.5 Å in response to EG solvation (Figure 4a), typically 20–40% of the 7 Å kaolin peak remains following EG solvation (Figure 4b). Similarly, formamide causes complete expansion of 10 Å and incomplete expansion of 7 Å peaks. Given that SEM observations revealed no hexagonal kaolinite, and that XRD analysis of randomly-oriented clays did not reveal peaks characteristic of kaolinite, incomplete expansion of 7 Å peaks probably reflects incomplete intercalation of halloysite by formamide (Churchman, 1990).

Halloysite transformations

The 10 Å to 7 Å transformation has been observed in experimental analyses (Brindley and Goodyear, 1948; Churchman and Carr, 1975; Churchman *et al.*, 1984) and in a climate with pronounced wet and dry seasons, where the shift from 10 Å to 7 Å halloysite is driven by soil desiccation during the dry season (Takahashi *et al.*, 1993). The 10 Å to 7 Å transition at La Selva is unusual in that it occurs across floodplains, terraces and residual soils of increasing age, and does not appear to be related to wet-dry cycles. Major element concentrations and particle-size distributions also exhibit pronounced changes across these topographic boundaries, particularly between floodplains and terraces (Table 3, Figure 1). The 10 Å to 7 Å halloysite transformations, soil chemical composition and particle-size trends appear to correlate with three distinct episodes of landscape change as described by Alvarado (1990), Nieuwenhuyse and van Breemen (1997) and Nieuwenhuyse *et al.* (2000), including (1) prolonged weathering of Pleistocene lava flows that emanated from the Cordillera Central, (2) subsequent incision and terrace formation during the late Pleistocene and Holocene epochs, and (3) renewed incision in the late Holocene and current development of 1–2, 10 and 100 y floodplains. Given that the soils at La Selva do not experience seasonal drying, and that the soils are perennially moist with no systematic variation in moisture content from floodplain to terrace and residual soils (Sollins *et al.*, 1994), the 10 Å to 7 Å transformation is probably not driven by seasonal variability in the water table, but rather by kinetic and/or thermodynamic controls.

The presence of halloysite in La Selva soils as old as 10–100 ky raises some interesting points about the stability of both 10 Å and 7 Å halloysite. Particularly intriguing is the nearly exclusive presence of 10 Å halloysite (relative to 7 Å halloysite) in soils on 1, 10 and 100 y floodplains, as well as its persistence in Pleistocene terrace soils. This implies greater stability of the 10 Å form than previously documented. Some

studies indicate that the 10 Å form is unstable, always transforming to 7 Å halloysite via dehydration with age (Churchman and Carr, 1975). Conversely, other studies document the "retrograde" transformation of kaolinite to 10 Å halloysite (Robertson and Eggleton, 1991; Singh and Gilkes, 1992), implying that 10 Å halloysite is stable or metastable under conditions that include water saturation, aqueous tetrahedrally coordinated Al (Merino *et al.*, 1989) and approximately 1:1 ratio of aqueous Al:Si. The perennially moist soil conditions of the study area are probably responsible for preservation of 10 Å halloysite. With no soil dessication, the 10 Å to 7 Å transformation is presumably controlled by kinetic factors for which rates are very low.

There is no evidence for transformation of 7 Å halloysite to kaolinite with increasing age. Halloysite has been described as kinetically favored and metastable (Jeong, 1998) as compared to thermodynamically stable kaolinite (Churchman and Carr, 1975; Jeong, 1998), but the fact that halloysite forms via kaolinite dissolution suggests that halloysite is stable relative to kaolinite given suitable conditions (Singh and Gilkes, 1992). From examination of particle-size distributions, ICP-AES, QXRD and SEM data, it appears that weathering rapidly reaches a quasi-steady-state at La Selva. Considering that kinetic factors are often more important than thermodynamic factors in governing soil reactions, particularly those among secondary minerals (McBride, 1994), quasi-steady-states may reflect slow reaction rates of metastable halloysite precursors to thermodynamically stable kaolinite, or that halloysite is thermodynamically stable in some soils (Robertson and Eggleton, 1991; Singh and Gilkes, 1992).

Nature and significance of a 14 Å dioctahedral mineral

Dioctahedral smectite, vermiculite, chlorite and interstratifications of these components occur in volcanic ash soils from numerous localities in Japan (Masui and Shoji, 1969; Tokashiki and Wada, 1975). Masui and Shoji (1969) studied numerous volcanic ash soil profiles and found that C horizons contain expandable 14 Å clay that passes upwards into dioctahedral vermiculite. This was interpreted to indicate vermiculite formation via chemical weathering of ash, particularly mica, amphibole, pyroxene and volcanic glass, with expandable clay a common vermiculite precursor (Masui and Shoji, 1969; Tokashiki and Wada 1975). Others (Pevear *et al.*, 1982; Nieuwenhuyse and van Breemen, 1997) have reported on expandable 14 Å clays in ash that formed by hydrothermal alteration prior to eruption, indicating that the expandable 14 Å clay (and 10 Å halloysite) in the youngest floodplain may have been transported into the soil by fluvial processes. Lack of expandable 14 Å clay in older floodplain and terrace soils, where dioctahedral vermiculite occurs, suggests transformation from dioctahedral smectite to dioctahedral vermiculite with time and leaching.

Bulk chemical composition

Depletion trends for Ca, Na, K and Si, and enrichment of Fe, Al and Ti are typical for highly weathered soils (Drever, 1997). Bulk chemical analysis indicates that Mg is being retained in the soil to a greater extent than Ca and Na (Table 4). The Mg oxide content in dioctahedral vermiculite and chlorite varies widely, from negligible to 10.14% (Newman and Brown, 1987), indicating that Mg at La Selva may be retained in hydroxide sheets of dioctahedral vermiculite. The Mg may also be retained by substitution for Fe in hydroxides and oxides (McBride, 1994). Primary minerals such as pyroxene and volcanic glass are not responsible for Mg retention in soils on terraces given their rapid dissolution rates and their virtual absence from the terrace soils.

Short-range order materials

Quantification of short-range order material is important because of its high anion exchange capacity and because of its relationship to other solid and aqueous phases in soil weathering environments. The presence of such materials at La Selva is indicated by three series of data. The QXRD data indicate that the total crystalline mineral content is 70–95%, thus implying that 5–30% of the soil is X-ray amorphous. Selective extraction using ammonium oxalate indicates that these soils contain 8–30% amorphous or short-range order materials. Normative calculations result in higher percentages of halloysite than are indicated by QXRD, with Al_2O_3 calculations providing the greatest difference (Table 3). This indicates that Al_2O_3 is more abundant than SiO_2 in the amorphous material, a finding that is verified by ICP-AES analysis of the ammonium oxalate extractant (Table 2). Furthermore, these findings are consistent with studies by Tan *et al.* (1975) and Nieuwenhuyse and van Breemen (1997), who found that Holocene and Pleistocene soils of similar climate, parent material and composition in eastern Costa Rica contain 20–27% amorphous solids.

The Al:Si ratios of 0.92–1.23 in the floodplain soils indicate that the short-range order material is allophane. This is in agreement with the findings of Jongmans *et al.* (1995), who documented allophanic amorphous material in an 18 ky old Andisol in eastern Costa Rica with Al:Si ratios ranging from 1 to 5. Five of the eight terrace and residual soils exhibit Al:Si ratios >5, which probably reflects the formation of amorphous Al hydroxide via leaching of Si from allophane (Jongmans *et al.*, 1995).

CONCLUSIONS

The dominant weathering sequence in these soils consists of (1) rapid dissolution of plagioclase and other primary minerals, and (2) pedogenic transformation of 10 Å halloysite and allophane to 7 Å halloysite and X-ray amorphous Al hydroxides. The shift from 10 Å to 7 Å halloysite appears to be age related. The 10 Å form

predominates in active floodplains and the 7 Å form predominates in residual soils formed atop Pleistocene lava flows. Intermediate-aged terraces consist of subequal amounts of the 10 Å and 7 Å forms.

An additional consideration is that of the prolonged persistence of both forms of halloysite, where the weathering of primary minerals and development of halloysite quickly reaches a quasi-steady-state. In this case, initial weathering of plagioclase feldspar is matched by the formation of allophane and 10 Å halloysite that appears to persist in a metastable state for thousands of years. The 7 Å form found at La Selva in Pleistocene soils indicates prolonged persistence in this environment.

Dioctahedral vermiculite is ubiquitous and appears to form via transformation from high-charge dioctahedral smectite. Preferential retention of Mg over Na and Ca in La Selva soils is linked to its retention in dioctahedral vermiculite and possible substitution for Fe in hydroxides.

REFERENCES

Agbu, P.A., Jones, R.L. and Ahmad, N. (1990) Mineralogy and weathering of a Trinidad Ultisol developed in porcellanite, *Soil Science*, **149**, 272–279.

Alvarado, G. (1990) Caracteristicas geologicas de la Estacion Biologica La Selva, Costa Rica. *Tecnología en Marcha*, **10**, 11–22.

Barshad, I. (1966) The effect of a variation in precipitation on the nature of clay mineral formation in soils from acid and basic igneous rocks. *Proceedings of the International Clay Conference, Jerusalem,* 167–173.

Bestland, E.A., Retallack, G.J. and Swisher, C.C., III (1997) Stepwise climate change recorded in Eocene-Oligocene sequences from central Oregon. *Journal of Geology,* **105**, 153–172.

Birkeland, P.W. (1969) Quaternary paleoclimatic implications of soil clay mineral distribution in a Sierra Nevada-Great Basin transect. *Journal of Geology,* **77**, 289–302.

Brindley, G.W. and Brown, G. (1980) *Crystal Structures of Clay Minerals and their X-ray Identification*. Monograph **5**. Mineralogical Society, London.

Brindley, G.W. and Goodyear, J. (1948) The transition of halloysite to metahalloysite in relation to relative humidity. *Mineralogical Magazine,* **28**, 407–422.

Calvert, C.S., Buol, S.W. and Weed, S.B. (1980) Mineralogical characteristics and transformations of a vertical rock-saprolite-soil sequence in the North Carolina Piedmont: II. Feldspar alteration – their transformations through the

profile. *Soil Science Society of America Journal,* **44**, 1104–1112.

Chukhrov, F.V. and Zvyagin, B.B. (1966) Halloysite: a crystallochemically and mineralogically distinct species. *Proceedings of the International Clay Conference, Jerusalem,* 11–25.

Churchman, G.J. (1990) Relevance of different intercalation tests for distinguishing halloysite from kaolinite in soils. *Clays and Clay Minerals,* **38**, 591–599.

Churchman, G.J. and Carr, R.M. (1975) The definition and nomenclature of halloysites. *Clays and Clay Minerals,* **23**, 382–388.

Churchman, G.J., Aldridge, L.P. and Carr, R.M. (1972) The relationship between hydrated and dehydrated states of an halloysite. *Clays and Clay Minerals,* **20**, 241–246.

Churchman, G.J., Whitton, J.S., Claridge, G.C.C. and Theng, B.K.G. (1984) Intercalation method using formamide for differentiating halloysite from kaolinite. *Clays and Clay Minerals,* **32**, 241–248.

Costanzo, P.M. and Giese, R.F. (1985) Dehydration of synthetic hydrated kaolinites; a model for the dehydration of halloysite (10 Å). *Clays and Clay Minerals,* **33**, 415–423.

Delvaux, B., Herbillon, A.J., Vielvoye, L. and Mestdagh, M.M. (1990) Surface properties and clay mineralogy of hydrated halloysitic soil clays. II: Evidence for the presence of halloysite/smectite (H/Sm) mixed-layer clays. *Clay Minerals,* **25**, 141–160.

Drever, J.I. (1973) The preparation of oriented clay mineral specimens for X-ray diffraction analysis by a filter membrane peel technique. *American Mineralogist,* **58**, 553–554.

Drever, J.I. (1997) *The Geochemistry of Natural Waters: Surface and Groundwater Environments.* Prentice Hall, Upper Saddle River, New Jersey, 436 pp.

Eswaran, H. and Wong, C.B. (1978) A study of a deep weathering profile on granite in peninsular Malaysia: III. Alteration of feldspars. *Soil Science Society of America Journal,* **42**, 154–158.

Grieve, I.C., Proctor, J. and Cousins, S.A. (1990) Soil variation with altitude on Volcan Barva, Costa Rica. *Catena,* **17**, 525–534.

Hillier, S. (1999) Use of an air brush to spray dry samples for X-ray powder diffraction. *Clay Minerals,* **34**, 127–135.

Hillier, S. and Ryan, P.C. (2002) Identification of halloysite (7 Å) by ethylene glycol solvation: the 'MacEwan effect'. *Clay Minerals,* **37**, 487–496.

Hughes, J.C. (1980) Crystallinity of kaolin minerals and their weathering sequence in some soils from Nigeria, Brazil, and Colombia. *Geoderma,* **24**, 317–325.

Jackson, M.L. (1964) Chemical composition of soils. Pp. 71–141 in: *Chemistry of the Soil* (F.E. Bear, editor). Reinhold, New York.

Janzen, D.H., editor (1983) *Costa Rican Natural History.* University of Chicago Press, USA.

Jeong, G.Y. (1998) Formation of vermicular kaolinite from halloysite aggregates in the weathering of plagioclase. *Clays and Clay Minerals,* **46**, 270–279.

Jongmans, A.G., Verburg, P., Nieuwenhuyse, A. and van Oort, F. (1995) Allophane, imogolite, and gibbsite in coatings in a Costa Rican Andisol. *Geoderma,* **64**, 327–342.

MacEwan, D.M.C. (1948) Complexes of clays with organic compounds I. Complex formation between montmorillonite and halloysite and certain organic liquids. *Transactions of the Faraday Society,* **44**, 349–367.

Masui, J. and Shoji, S. (1969) Crystalline clay minerals in volcanic ash soils of Japan. *Proceedings of the International Clay Conference, Tokyo,* 383–392.

McBride, M.B. (1994) *Environmental Chemistry of Soils.* Oxford University Press, New York, 406 pp.

Merino, E., Harvey, C. and Murray, H.H. (1989) Aqueous-chemical control of the tetrahedral-aluminum content of quartz, halloysite, and other low-temperature silicates. *Clays and Clay Minerals,* **37**, 135–142.

Mizota, C. and Van Reeuwijk, L.P. (1989) *Clay Mineralogy and Chemistry of Soils Formed in Volcanic Material in Diverse Climatic Regions.* Soil Monograph, **2**. International Soil Reference and Information Centre, Wageningen, Netherlands, 185 pp.

Moore, D.M. and Reynolds, R.C. Jr (1997) *X-ray Diffraction and the Identification and Analysis of Clay Minerals.* Oxford University Press, New York, 378 pp.

Nagasawa, K. (1978) Kaolin minerals. Pp. 189–215 in: *Clays and Clay Minerals of Japan* (T. Sudo and S. Shimoda, editors). Developments in Sedimentology, **26**. Elsevier, Amsterdam.

Newman, A.C.D and Brown, G. (1987) The chemical constitution of clays. Pp. 1–129 in: *Chemistry of Clays and Clay Minerals* (A.C.D. Newman, editor). Monograph **6**. Mineralogical Society, London.

Nieuwenhuyse, A. and van Breemen, N. (1997) Quantitative aspects of weathering and neoformation in selected Costa Rican volcanic soils. *Soil Science Society of America Journal,* **61**, 1450–1458.

Nieuwenhuyse, A., Verburg, P.S.J. and Jongmans, A.G. (2000) Mineralogy of a soil chronosequence on andesitic lava in humid tropical Costa Rica. *Geoderma,* **98**, 61–82.

Parham, W.E. (1969) Formation of halloysite from feldspar; low temperature, artificial weathering versus natural weathering. *Clays and Clay Minerals,* **17**, 13–22.

Parfitt, R.L., Saigusa, M. and Cowie, J.D. (1984) Allophane and halloysite formation in a volcanic ash bed under different moisture conditions. *Soil Science,* **138**, 360–364.

Pevear, D.R., Dethier, D.P. and Frank, D. (1982) Clay minerals in the 1980 deposits from Mount St. Helens. *Clays and Clay Minerals,* **30**, 241–252.

Quantin, P., Balesdent, J., Bouleau, A., Delaune, M. and Feller, C. (1991) Premiers stades d'altèration de ponces volcaniques en climat tropical humide (Montagne Pelèe, Martinique). *Geoderma,* **50**, 125–148.

Retallack, G.J. (1983) Eocene and Oligocene paleosols from Badlands National Park, South Dakota. *Geological Society of America, Special Paper,* **193**, 82 pp.

Righi, D., Terribile, F. and Petit, S. (1999) Pedogenic formation of kaolinite-smectite mixed layers in a soil toposequence developed from basaltic parent material in Sardinia (Italy). *Clays and Clay Minerals,* **47**, 505–514.

Robertson, I.D.M. and Eggleton, R.A. (1991) Weathering of granitic muscovite to kaolinite and halloysite and of plagioclase-derived kaolinite to halloysite. *Clays and Clay Minerals,* **39**, 113–126.

Singh, B. and Gilkes, R.J. (1992) An electron-optical investigation of the alteration of kaolinite to halloysite. *Clays and Clay Minerals,* **40**, 212–229.

Sollins, P., Sancho, M., Mata, R. and Sanford, R.L., Jr (1994) Soils and soil process Research. Pp. 34–53 in: *La Selva: Ecology and Natural History of a Neotropical Rain Forest* (L.A. McDade, K.S. Bawa, H.A. Hespenheide, and G.S. Hartshorn, editors). University of Chicago Press, Chicago.

Starkey, H.C., Blackmon, P.D. and Hauff, P.L. (1984) The routine mineralogical analysis of clay-bearing samples. *United States Geological Survey Bulletin,* **1563**, 32 pp.

Takahashi, T., Dahlgren, R. and van Susteren, P. (1993) Clay mineralogy and chemistry of soils formed in volcanic materials in the xeric moisture regime of Northern California. *Geoderma,* **59**, 131–150.

Tan, K.H., Perkins, H.F. and McCreery, R.A. (1975) Amorphous and crystalline clays in volcanic ash soils of Indonesia and Costa Rica. *Soil Science,* **119**, 431–440.

Tokashiki, Y. and Wada, K. (1975) Weathering implications of the mineralogy of clay fractions of two ando soils, Kyushu. *Geoderma*, **14**, 47–62.

Wada, K. (1989) Allophane and imogolite. Pp. 1051–1087 in: *Minerals in Soil Environments (2nd edition)* (J.B. Dixon and S.B. Weed, editors). Soil Science Society of America Book Series **1**, Madison, Wisconsin.

Watanabe, T., Sawada, Y., Russell, J.D., McHardy, W.J. and Wilson, M.J. (1992) The conversion of montmorillonite to interstratified halloysite-smectite by weathering in the Omi acid clay deposit, Japan. *Clay Minerals,* **27**, 159–173.